Learning robotic needle steering from inverse finite element simulations

(Workshop Paper)

Pedro Henrique Suruagy Perrusi
ICube laboratory
University of Strasbourg
Strasbourg, France
phsuruagyperrusi@unistra.fr

Anna Cazzaniga
Nearlab laboratory
Politecnico Di Milano
Milan, Italy
anna.cazzaniga@mail.polimi.it

Paul Baksic
ICube laboratory
University of Strasbourg
Strasbourg, France
p.baksic@unistra.fr

Eleonora Tagliabue
Altair Robotics laboratory
University of Vernona
Verona, Italy
eleonora.tagliabue@univr.it

Elena De Momi
Nearlab laboratory
Politecnico Di Milano
Milan, Italy
elena.demomi@polimi.it

Hadrien Courtecuisse
ICube laboratory
University of Strasbourg
Strasbourg, France
hcourtecuisse@unistra.fr

***Abstract*—Tissue motion compensation during robotic needle steering is a challenging research topic. While the deformable non-linear coupling between needle and tissue is captured by simulation-based control strategies, they increase significantly the computational cost of the control. In this work, we rely on machine learning methods to enable autonomous robotic needle steering with very low computation times. We propose to use an Extreme Learning Machine (ELM) to learn an inverse model which accounts for needle-tissue interaction. The ELM trains with synthetic data generated from multiple needle insertions controlled by inverse finite-element simulations. Results indicate the method is able to achieve clinical compatible precision, and it's robust to previously unseen trajectory-shapes and variable tissue elasticity parameters, while using only a third of the computational time demanded for simulation-based methods.**

***Index Terms*—percutaneous procedures, deformable needle steering, data-driven methods**

I. Introduction

Percutaneous needle insertion procedures are popular medical interventions because they minimize the patient trauma reducing his/her recovery time. Although these procedures are generally performed manually, they remain challenging because they require a high targeting accuracy in a deformable environment. Liver procedures are specially challenging given its elasticity. In fact, physicians need for robotic assistance in these procedures has been reported [1].

Many studies have proposed robotic assistance to needle steering [2]. Some works target the robot-assisted needle steering problem using simplified models that do not include needle-tissue interactions. They are efficient and fast enough to meet the robotic control time requirements, but they have a low accuracy [3] due to the fact that non-linearity of the needle-tissue interactions are not modelled.

This work was supported by French National Research Agency (ANR) within the project SPERRY ANR-18-CE33-0007 and the Investissements d'Avenir program (ANR-11-LABX-0004, Labex CAMI). Conflict of interest: Authors state no conflict of interest.

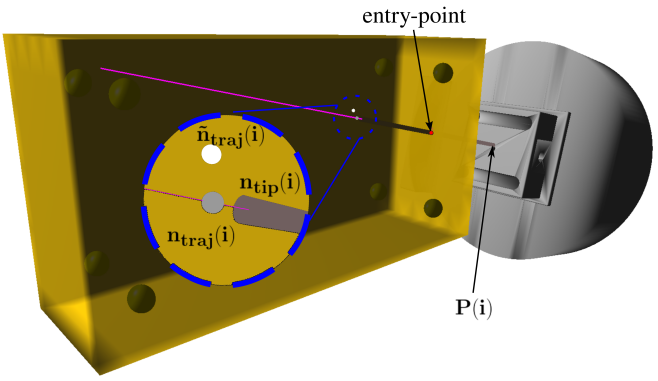

Fig. 1. Example of a FE simulation of a needle insertion through an entry-point along a linear trajectory. For a given time-step i, figure shows the robot position $\mathbf{P}(i)$, needle tip position $\mathbf{n_{tip}}(i)$, trajectory point $\mathbf{n_{traj}}(i)$ sliding trough the pink trajectory. After noise addition, a modified target point $\tilde{\mathbf{n}}_{\mathbf{traj}}(i)$ is also shown in the image.

In order to account for this complex behavior, a physics-based simulation can be integrated into the control loop to estimate tissue deformations caused by the needle motion. In particular, methods that use a finite element simulation to compute the inverse kinematics of deformable needle (denoted here as inverse finite element method I-FEM) have been able to reach a sub-milimetric precision in aiming target located deep inside soft tissues. [4]–[6]. These methods however require high computational cost and thus introduce delay in the robotic command, reducing its stability. Only after significant computational time reduction, the method is able to perform stable needle insertions under external perturbations (simulated respiratory motion) [6].

In this paper, we propose to use Machine Learning (ML) to control the needle movements while performing a needle insertion. In a previous preliminary analysis [7], we have showed

that Extreme Learning Machines (ELM) neural networks are able to learn from I-FEM and provide robotic commands at a faster rate. The idea of training ML methods with synthetic data generated from highly accurate finite element simulations has been recently investigated in many works, to tackle the lack of patient data which usually characterizes the medical domain [8]–[10]. This paper presents an extended description of the method and explores the solution robustness to variable tissue elasticity parameters and different trajectory shapes.

II. Background

Introduced in [4], the I-FEM method is able to compensate for tissue deformation by including a FE simulation into the control loop. The needle insertion problem is formulated as a minimization of the objective function $\mathbf{e}$. The needle tissue interaction imposes a non-linear relationship between $\mathbf{e}$ and the robot end-effector pose $(\mathcal{X})$. The FE simulation is then used to linearize this relationship computing the so-called *Jacobian of the simulation*:

$$\mathbf{J}\Delta\mathcal{X} = \Delta\mathbf{e} \tag{1}$$

An end-effector reference $\mathbf{T}$ can then be computed as a solution to the linearized inverse problem:

$$\mathbf{T} = \mathcal{X} - \mathbf{J}^{\dagger}(\mathbf{k} \odot \mathbf{e}) \tag{2}$$

where $\mathbf{J}^{\dagger}$ is a damped pseudo-inverse of $\mathbf{J}$, $\odot$ is the Hadamard product and $\mathbf{k}$ is a gain vector for weighting each objective function separately (see [6] for details).

The number of objective functions may vary along the needle insertion given the current state of the procedure, either inside or outside the tissue. In this study, only solutions for when the needle is inside will be addressed, since they're the most challenging. A first objective

$$\mathbf{e_p} = \mathbf{n_{traj}} - \mathbf{n_{tip}} \tag{3}$$

minimizes the error between the needle tip position $\mathbf{n_{tip}}$ and a target position that moves along a pre-defined trajectory $\mathbf{n_{traj}}$ as seen in Figure 1. Other two objectives enforce a remote-center-of-motion (RCM) at the level of the insertion point to prevent tissue damage. Because these are not useful for the comprehension of the paper contribution, they will not be further explained. For more precision see [6].

III. Methods

In this study, synthetic data extracted from multiple I-FEM simulations is used to train an ELM neural network to perform needle steering in deformable tissues. For the sake of simplicity, in this work we assume that the entry-point position is a-priori known and fixed. While the I-FEM uses two additional objective functions to avoid tissue damage at the entry-point, it is not expected that the ELM solves for these objectives. Instead, a RCM is imposed to the needle, by automatically computing the end-effector orientation required to make the needle go through the initial entry point position.

A. Dataset Generation

A database of multiple I-FEM needle insertion simulations into a rectangular geometry of dimensions $36 \times 62 \times 122mm$ is used to train the ELM neural network. To generate the trajectories, which are straight, we consider a regular XY grid at $Z = 122\,\mathrm{mm}$ composed of 105 points equally spaced along the XY surface. Each point in the grid corresponds to the end point of a different trajectory, while the initial point is always the same (the fixed entry point). Figure 1 presents an overview of an example simulation.

At each simulation time-step, sample data described in Table I are exported and from each trajectory more than 10^4 samples can be generated. After the samples extraction, we conduct a performances analysis to choose the optimal database size which has been found out to be $N = 10^4$ samples with 90% of them in the train set and 10% of them in the test set.

In order to prevent over-fitting, some variability is introduced in the target position such that the network has the possibility to learn how to compensate for possible bigger mismatches between $\mathbf{n_{tip}}(i)$ and $\mathbf{n_{traj}}(i)$. Uniform noise $\tilde{\mathbf{u}}(i)$ between $\pm 0.25mm$ is added to the trajectory target position: $\widetilde{\mathbf{n}}_{\mathbf{traj}}(i) = \mathbf{n_{traj}}(i) + \tilde{\mathbf{u}}(i)$. This perturbed position is used as the input of the I-FEM method, its objective function is thus $\widetilde{\mathbf{e}}_{\mathbf{p}}(i) = \widetilde{\mathbf{n}}_{\mathbf{traj}}(i) - \mathbf{n_{tip}}(i)$.

TABLE I
Variables exported from each simulation time-step i directly (top) and derived (bottom).

Symbol	Description
$\mathbf{P}(i)$	Robotic end-effector position
$\mathbf{T}(i)$	Target pose commanded by I-FEM
$\mathbf{n}(i)$	Needle tip position
$\tilde{\mathbf{n}}_{\mathbf{traj}}(i)$	Trajectory target point position with uniform noise
$\Delta\mathbf{P}(i)$	3D position displacement to reach $\mathbf{T}(i)$ from $\mathbf{P}(i)$
$\widetilde{\mathbf{e}}_{\mathbf{p}}(i)$	3D distance vector between $\widetilde{\mathbf{n}}_{\mathbf{traj}}(i)$ and $\mathbf{n}(i)$

Thus, the I-FEM model is used to compute the target command $\mathbf{T}$ to place the needle tip in correspondence with the desired $\widetilde{\mathbf{n}}_{\mathbf{traj}}(\mathbf{i})$ with constant operational space velocity of $1\,\mathrm{cm\,s^{-1}}$. The tissue's parameters were set to mimic the human liver, with a Young Modulus (YM) of $6.3kPa$ and a Poisson ratio of 0.4. FE models use linear co-rotational formulation of elasticity [11]. The needle is modeled as serially linked beam-elements following Timoshenko's formulation. The needle-tissue FE interaction follows a Lagrange constraint formulation [12]. A similar setup was validated in simulation and during a physical experiments [5].

B. Neural Network Architecture

Inspired by analogous applications in different fields of medical robotics [13] [14], the ELM is a viable model to learn the non-linear relationship between robot position and needle tip target. It is a feed forward neural network with a single hidden layer:

$$\mathbf{H} = g(\mathbf{wX} + \mathbf{b}) \tag{4}$$

$$\mathbf{H}\boldsymbol{\beta} = \mathbf{Y} \tag{5}$$

Where $g()$ is the activation function, $\mathbf{w}$ is the input layer weights matrix, $\mathbf{X}$ are the neural network inputs, $\mathbf{b}$ is the vector of the biases summed to the hidden neurons, $\boldsymbol{\beta}$ is output layer weights matrix and $\mathbf{Y}$ are the neural network outputs. The only hyper-parameters to consider are $\boldsymbol{M}$ number of nodes in the hidden layer and the type of activation-function. In this study it is implemented with $\boldsymbol{M = 25}$ and sigmoid activation functions. For an $\boldsymbol{i}$'th sample, model inputs are the robot end-effector 3D position $\mathbf{P}(\boldsymbol{i})$ and the tip to target objective $\mathbf{e_p}(\boldsymbol{i})$. The ELM is trained to map the inputs $\mathbf{x}(\boldsymbol{i}) = \begin{bmatrix}\mathbf{P}(\boldsymbol{i}) & \mathbf{e_p}(\boldsymbol{i})\end{bmatrix}^{\boldsymbol{T}}$ into 3D displacements of the robotic end-effector: $\mathbf{y}(\boldsymbol{i}) = [\boldsymbol{\Delta}\mathbf{P}(\boldsymbol{i})]$.

IV. Experiments and Results

A. Experiments

The experiments require the trained ELM to command the robot to steer the needle in a realistic FE simulation. In order to address if the ELM is capable of generalizing its predictions to previously unseen scenarios, two experiments are proposed.

In a first case, the ELM will be tested against 500 previously unseen trajectories, containing a set of $\mathbf{100}$ straight trajectories (LIN) and another set $\mathbf{400}$ curved trajectories (CUR). CUR trajectories were generated by applying a sinusoidal overlay to LIN trajectories in different directions of the global reference frame. A second experiment addresses the ELM robustness to different tissue properties. The ELM network is trained using samples related to a tissue with a constant YM of $\boldsymbol{6.3kPa}$. In this second experiment, instead, we test the model performances using tissues with a YM varying in the range of the human liver, from $\boldsymbol{5.5kPa}$ to $\boldsymbol{6.3kPa}$ [15]. Smaller YM implies more significant deformations which can lead to higher final errors.

B. Validation Protocol

As performance metrics, both the success rate and the tip to target root-mean square-error (RMSE) along the needle insertion will be considered. For a given trajectory interpolated in $\boldsymbol{N_p}$ target points, the root mean square error is defined as

$$\boldsymbol{RMSE_{tra}} = \sqrt{\frac{\sum_{i=0}^{N_p}(\mathbf{n_{tip}(i+1)} - \mathbf{n_{traj}(i)})^2}{\boldsymbol{N_p}}} \quad (6)$$

Another important metric is the success rate: $\boldsymbol{S} = {}^{N_s}/_{N_{traj}}$, where $\boldsymbol{N_{traj}}$ is the total number of trajectories and $\boldsymbol{N_s}$ is the number of cases in which the ELM is able to drive the needle without introducing instabilities in the simulation.

C. Results and Discussion

Both the ELM and the I-FEM are able to successfully perform the needle insertion along the 500 insertions of the LIN and CUR sets ($\boldsymbol{S_1 = 100\%}$). Their results are reported in Figure 2. Although I-FEM presents lower errors in the LIN set when compared to the ELM, this relationship is reversed for the CUR set, where the ELM is more precise. Statistical analysis comparing both $\boldsymbol{RMSE}$ sets rejects the hypothesis that both measurements come from a same distribution

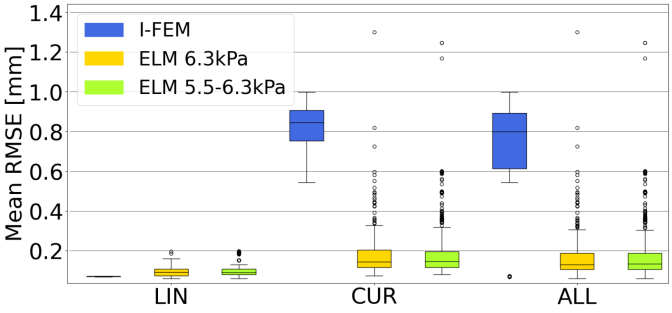

Fig. 2. Needle precision comparison along linear (LIN) and curved (CUR) trajectories and their union (ALL).

($\boldsymbol{p_{value} < 0.01}$, two-tailed sign test). This result indicates that the addition of uniform noise to $\mathbf{n_{traj}}$ at data generation time is able to prevent over-fitting and allows the ELM to generalize to previously unseen trajectories from both LIN and CUR sets.

In the second experiment, where YM changes, not all the trajectories are successfully followed. The ELM-driven simulation is stable for $\boldsymbol{S_2 = 98\%}$ of the trajectories. Failure cases are trajectories with end-points close to the tissue's borders, which is expected to be the most sensitive region for the model, since the training data is more sparse for these positions. Figure 2 presents quantitative results for the successful scenarios. Statistical analysis comparing the ELM performances when YM is constant or variable, cannot reject the null hypothesis that measurements come from distributions with same mean ($\boldsymbol{p_{value} > 0.05}$, Mann Whitney U test). Although no conclusions can be drawn on the significance of the results, Figure 2 shows that the results obtained with variable YM are aligned with those with constant YM, and outperform I-FEM on the CUR sets.

From the results it is clear that ELM precision is sub-millimetric along all the trajectories, thus compatible to clinical practice. A thorough comparison to I-FEM precision still needs to be addressed, since the ELM still does not solve for the needle orientation nor the entry-point RCM constraints, which are highly non-linear. For all the experiments the computational time advantage of the ELM is maintained, leading to an average reduction of $\mathbf{60\%}$ (see [7] for details).

V. Conclusions

The use of ELM to perform needle steering into soft tissue simulations presents promising perspectives. Results of both experiments show the method is stable and more precise than I-FEM for previously unseen curved trajectories. In future works the ELM will be adapted to fit scenarios with entry point variability, as it is only implicitly considered in the current formulation. A detailed comparison between I-FEM and the ELM including entry-point constraints and tissue stress will also be addressed. Finally, an experimental validation in an anatomical phantom will be performed to address the method's viability in physical scenarios.

REFERENCES

[1] T. L. De Jong, N. J. van de Berg, L. Tas, A. Moelker, J. Dankelman, and J. J. van den Dobbelsteen, "Needle placement errors: Do we need steerable needles in interventional radiology?," Medical Devices: Evidence and Research, vol. 11, pp. 259–265, 2018.

[2] F. J. Siepel, B. Maris, M. K. Welleweerd, V. Groenhuis, P. Fiorini, and S. Stramigioli, "Needle and Biopsy Robots: a Review," Current Robotics Reports, pp. 73–84, 2021. Publisher: Current Robotics Reports.

[3] R. J. Webster, J. S. Kim, N. J. Cowan, G. S. Chirikjian, and A. M. Okamura, "Nonholonomic modeling of needle steering," International Journal of Robotics Research, vol. 25, no. 5-6, pp. 509–525, 2006. ISBN: 0278364906065.

[4] Y. Adagolodjo, L. Goffin, M. De Mathelin, and H. Courtecuisse, "Inverse real-time Finite Element simulation for robotic control of flexible needle insertion in deformable tissues," IEEE International Conference on Intelligent Robots and Systems, vol. 2016-Novem, pp. 2717–2722, 2016. ISBN: 9781509037629.

[5] Y. Adagolodjo, L. Goffin, M. De Mathelin, and H. Courtecuisse, "Robotic Insertion of Flexible Needle in Deformable Structures Using Inverse Finite-Element Simulation," IEEE Transactions on Robotics, vol. 35, no. 3, pp. 697–708, 2019.

[6] P. Baksic, H. Courtecuisse, C. Duriez, and B. Bayle, "Robotic needle insertion in moving soft tissues using constraint-based inverse Finite Element simulation," ICRA 2020-IEEE International Conference on Robotics and Automation, pp. 1–7, 2020.

[7] P. H. S. Perrusi, A. Cazzaniga, P. Baksic, and E. Tagliabue, "Robotic needle steering in deformable tissues with extreme learning machines," in Proceedings of AUTOMED 2021, p. 3, 2021.

[8] A. Mendizabal, E. Tagliabue, T. Hoellinger, J.-N. Brunet, S. Nikolaev, and S. Cotin, "Data-Driven Simulation for Augmented Surgery," in Developments and Novel Approaches in Biomechanics and Metamaterials (B. E. Abali and I. Giorgio, eds.), pp. 71–96, Cham: Springer International Publishing, 2020.

[9] M. Pfeiffer, C. Riediger, S. Leger, J.-P. Kühn, D. Seppelt, R.-T. Hoffmann, J. Weitz, and S. Speidel, "Non-rigid volume to surface registration using a data-driven biomechanical model," in Medical Image Computing and Computer Assisted Intervention – MICCAI 2020 (A. L. Martel, P. Abolmaesumi, D. Stoyanov, D. Mateus, M. A. Zuluaga, S. K. Zhou, D. Racoceanu, and L. Joskowicz, eds.), (Cham), pp. 724–734, Springer International Publishing, 2020.

[10] E. Tagliabue, D. Dall'Alba, M. Pfeiffer, M. Piccinelli, R. Marin, U. Castellani, S. Speidel, and P. Fiorini, "Data-driven intra-operative estimation of anatomical attachments for autonomous tissue dissection," IEEE Robotics and Automation Letters, vol. 6, no. 2, pp. 1856–1863, 2021.

[11] F. Faure, C. Duriez, H. Delingette, J. Allard, B. Gilles, S. Marchesseau, H. Talbot, H. Courtecuisse, G. Bousquet, I. Peterlik, and S. Cotin, SOFA: A Multi-Model Framework for Interactive Physical Simulation. Springer, 2012.

[12] C. Duriez, C. Guébert, M. Marchal, S. Cotin, and L. Grisoni, "Interactive simulation of flexible needle insertions based on constraint models," Lecture Notes in Computer Science (including subseries Lecture Notes in Artificial Intelligence and Lecture Notes in Bioinformatics), vol. 5762 LNCS, no. PART 2, pp. 291–299, 2009. ISBN: 3642042708.

[13] W. Xu, J. Chen, H. Y. Lau, and H. Ren, "Data-driven methods towards learning the highly nonlinear inverse kinematics of tendon-driven surgical manipulators," International Journal of Medical Robotics and Computer Assisted Surgery, vol. 13, no. 3, pp. 1–11, 2017.

[14] R. A. Porto, F. Nageotte, P. Zanne, and M. De Mathelin, "Position control of medical cable-driven flexible instruments by combining machine learning and kinematic analysis," Proceedings - IEEE International Conference on Robotics and Automation, vol. 2019-May, pp. 7913–7919, 2019. ISBN: 9781538660263.

[15] D. Roulot, S. Czernichow, H. Le Clésiau, J.-L. Costes, A.-C. Vergnaud, and M. Beaugrand, "Liver stiffness values in apparently healthy subjects: Influence of gender and metabolic syndrome," Journal of Hepatology, vol. 48, pp. 606–613, Apr. 2008.